Available online at www.sciencedirect.com
SCIENCE DIRECT®
Journal of Power Sources 137 (2004) 206–215
JOURNAL OF POWER SOURCES
www.elsevier.com/locate/jpowsour

Simulation analysis of a system combining solid oxide and polymer electrolyte fuel cells

Masayuki Yokoo*, Tetsuo Take

NTT Energy and Environment Systems Laboratories, NTT Corporation, 3-1, Wakamiya, Morinosato, Atsugi-shi, Kanagawa 243-0198, Japan

Received 5 January 2004; accepted 7 June 2004
Available online 6 August 2004

Abstract

We evaluated the performance of system combining a solid oxide fuel cell (SOFC) stack and a polymer electrolyte fuel cell (PEFC) stack by a numerical simulation. We assume that tubular-type SOFCs are used in the SOFC stack. The electrical efficiency of the SOFC–PEFC system increases with increasing oxygen utilization rate in the SOFC stack. This is because the amount of exhaust heat of the SOFC stack used to raise the temperature of air supplied to it decreases as its oxygen utilization rate increases and because that used effectively as the reaction heat of the steam reforming reaction of methane in the stack reformer increases. The electrical efficiency of the SOFC–PEFC system at 190 kW ac is 59% (LHV), which is equal to that of the SOFC-gas turbine combined system at 1014 kW ac.

Keywords: Solid oxide fuel cell; Polymer electrolyte fuel cell; Combined system; Steam reforming reaction; Methane

1. Introduction

The electrical efficiency of a power generation system using a solid oxide fuel cell (SOFC) stack is expected to be very high [1]. An SOFC cogeneration system that generates electricity and heat used for heating water has achieved 46% (LHV) electrical efficiency at 109 kW ac [2]. However, it has been pointed out that an SOFC system that generates electricity in the SOFC stack and other generating equipment can provide higher electrical efficiency than the SOFC cogeneration system [1].

SOFC systems that generate electricity in an SOFC stack and gas turbine (GT) are receiving attention [3,4]. At 19.5 MW ac, the electrical efficiency of a SOFC–GT system is expected to reach 70% [3]. However, SOFC–GT systems are lauder than SOFC cogeneration systems, and the cost of the auxiliary equipment is higher. In addition, the energy conversion efficiency of the GT decreases as the output decreases, so at 220 kW ac the electrical efficiency of a SOFC–GT system using a 50 kW-class GT is expected to be 57% [4], which is far lower than that at 19.5 MW ac.

Systems that generate electricity in the SOFC stack and a polymer electrolyte fuel cell (PEFC) stack are also attracting attention [5,6]. The SOFC–PEFC system can provide higher efficiency than SOFC cogeneration systems [5,6] like the SOFC–GT system. The SOFC–PEFC system is quieter than the SOFC–GT system, and the cost of the auxiliary equipment is lower. The SOFC–PEFC systems can provide higher efficiency than the SOFC–GT systems when the output is comparatively small, because the efficiency of the PEFC stack remains almost constant even as the output decreases. However, the performance of the SOFC–PEFC system has not been clarified yet.

We quantitatively simulated and clarified the performance of a 200 kW-class SOFC–PEFC system with a 100 kW-class tubular SOFC stack.

2. Simulation models

2.1. SOFC stack

The SOFC stack consists of 1152 stack units, each of which consists of a tubular SOFC, stack reformer, pre-reformer, and combustor as shown in Fig. 1. The tubular SOFC is composed of the anode, cathode, and solid oxide

* Corresponding author. Fax: +81-46-270-2702.
E-mail address: m.yokoo@aecl.ntt.co.jp (M. Yokoo).

0378-7753/$ – see front matter © 2004 Elsevier B.V. All rights reserved.
doi:10.1016/j.jpowsour.2004.06.007

Nomenclature

A	heat transfer area (m^2)
C	isopiestic specific heat (J/mol K)
d	thickness (m)
E	electromotive force (V)
F	Faraday's constant (C/mol)
h	heat transfer coefficient (W/m^2 K)
J	current density (A/m^2)
K	equilibrium constant
l	length (m)
L_o	energy loss ratio to gross ac output
M	molar flow rate (mol/s)
M_a	molar flow rate of anode exhaust gas from tubular SOFC at minimum oxygen utilization rate to keep T_m at setting temperature (mol/s)
N	number of tubular SOFCs in SOFC stack
N_u	non-dimensional heat transfer coefficient
p	partial pressure (Mpa)
Q	radiation loss from 100 kW class SOFC stack made by SWPC (W)
R	gas constant (J/mol K)
R_B	base resistance ($\Omega\,m^2$)
R_c	contact resistance between each tubular SOFC ($\Omega\,m^2$)
R_e	summation of anode, cathode, and electrolyte resistance of tubular SOFC ($\Omega\,m^2$)
S	cross-sectional area (m^2)
T	temperature (K)
T_h	temperature for definition of enthalpy change (K)
T_m	maximum temperature in tubular SOFC (K)
U_f	fuel utilization rate (%)
U_o	oxygen utilization rate (%)
V	cell voltage (V)
V_p	volume of pre-reformer (m^3)
W	ac output (W)
x	coordinate along gas flow (m)

Greek letters

ΔH	enthalpy change at T_{BASE} (J/mol)
ψ	dc/ac conversion efficiency
δ	internal diameter (m)
ε	activation energy (J/mol)
ϕ	ohmic overpotential of tubular SOFC (V)
η	electrical efficiency (%)
φ	external diameter (m)
κ	frequency factor ($mol/(m^3/cat)s\,MPa^{0.9845}$)
λ	heat conductivity (W/m K)

Subscript

A	air
AEG	anode exhaust gas
ac	alternating current
ALM	alumina tube
AMB	ambient
ANO	anode of tubular SOFC
APE	anode exhaust gas for PEFC stack
AUX	auxiliary machine
AVE	average
BLOW	air blower
CATH	cathode of tubular SOFC
CEG	combustion exhaust gas
CELL	anode, cathode, and electrolyte assembled solid
COM	combustor
dc	direct current
ELE	electrolyte
F	fuel
FCHA	fuel channel
HE	heat exchanger
IN	inlet
INS	inside
OTHER	other than air blower
OUT	outlet
OUTS	outside
OXI	oxidation
PE	PEFC
PEstack	PEFC stack
PRE	pre-reformer
REC	recycled gas for steam reforming
SHIF	shift reaction
SO	tubular SOFC
SOstack	SOFC stack
SR	steam reforming reaction
SRE	stack reformer
SYS	SOFC–PEFC system
Wall	wall

electrolyte. We refer the anode, cathode, and electrolyte assembled solid as the cell in this paper. The tubular SOFCs are electrically connected to each other through Ni felt in the SOFC stack [7]. The methane fed to the stack unit is mixed with the recycle gas for steam reforming and supplied to the pre-reformer. Some of the methane is converted to hydrogen and carbon monoxide by the steam reforming reaction in the pre-reformer. The exhaust gas from the pre-reformer is supplied to the stack reformer, where the residual methane is converted to hydrogen and carbon monoxide by the steam reforming reaction using the exhaust heat of the tubular SOFC as the reaction heat. The exhaust gas from the stack reformer is supplied to the an-

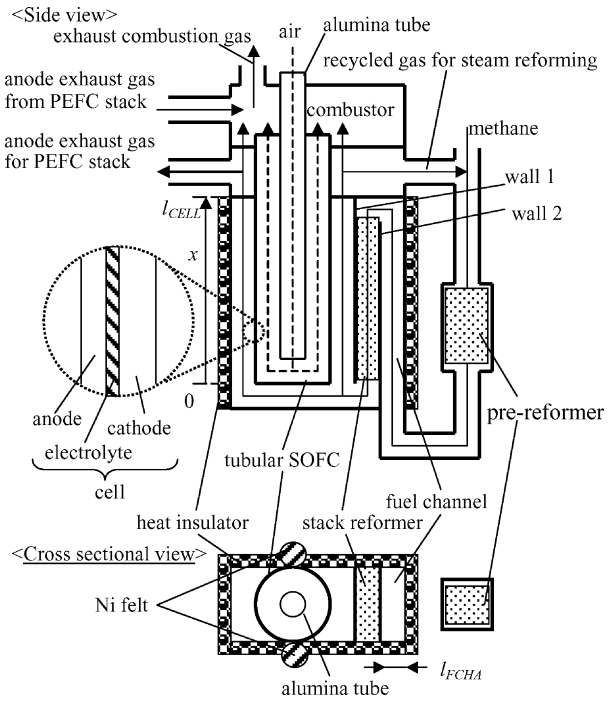

Fig. 1. Stack unit.

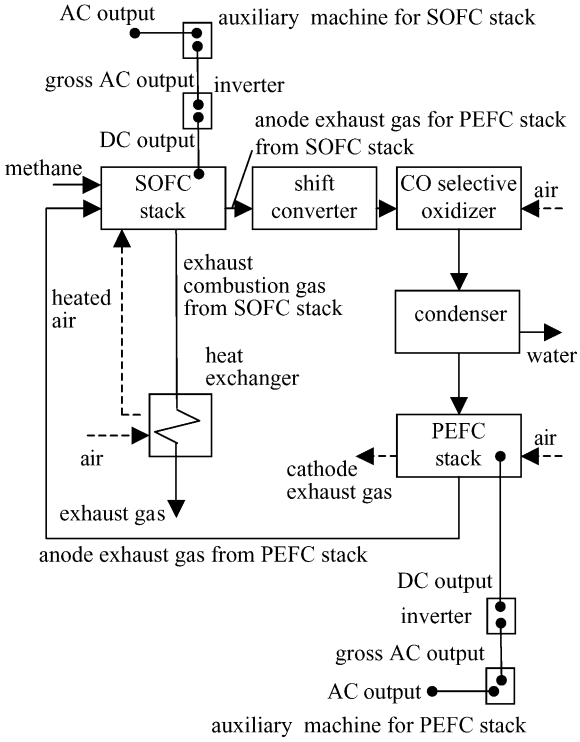

Fig. 2. SOFC–PEFC system.

ode of the tubular SOFC and used for power generation. A part of the anode exhaust gas is discharged from the stack unit as the anode exhaust gas for the PEFC stack. All anode exhaust gases for the PEFC stack from the stack units are gathered and supplied to the shift converter as the anode exhaust gas for the PEFC stack from the SOFC stack (see Fig. 2). Another part of the anode exhaust gas from the tubular SOFC is recycled to the pre-reformer as the recycle gas for steam reforming. We chose a molar flow rate of the recycle gas for steam reforming so that the steam to methane molar ratio (S/C ratio) in the gas supplied to the pre-reformer is 3.0. The rest of the anode exhaust gas from the tubular SOFC is fed to the combustor together with the anode exhaust gas from the PEFC stack and the cathode exhaust gas from the tubular SOFC. The methane, hydrogen, and carbon monoxide in the two anode exhaust gases completely react with the oxygen in the cathode exhaust gas from the tubular SOFC in the combustor. All combustion exhaust gases from the combustors of the stack units are gathered and fed to the heat exchanger as the combustion exhaust gas from the SOFC stack (see Fig. 2). The air is fed to the alumina tube installed inside the tubular SOFC, and the temperature of the air is raised by using the exhaust heat of the tubular SOFC. The heated air is supplied to the cathode of the tubular SOFC and used for power generation.

We used the following assumptions for the simulation of the SOFC stack.

(1) The methane, air, and anode exhaust gas from the PEFC stack fed to the SOFC stack are distributed to every stack unit equally.

(2) Both the steam reforming reaction of methane,

$$CH_4 + H_2O \rightarrow CO + 3H_2, \quad (1)$$

and the shift reaction,

$$CO + H_2O \leftrightarrow CO_2 + H_2, \quad (2)$$

occur in the pre-reformer and stack reformer. The shift reaction is in thermodynamic equilibrium in both the pre-reformer and stack reformer [8].

(3) The oxidation of hydrogen,

$$H_2 + \tfrac{1}{2}O_2 \leftrightarrow H_2O, \quad (3)$$

the oxidation of carbon monoxide,

$$CO + \tfrac{1}{2}O_2 \leftrightarrow CO_2, \quad (4)$$

and the oxidation of methane,

$$CH_4 + 2O_2 \leftrightarrow 2H_2O + CO_2, \quad (5)$$

occur in the tubular SOFC as cell reactions. These oxidations are in thermodynamic equilibrium at the anode side of the tubular SOFC [9].

(4) The temperature profiles of the anode, cathode, and electrolyte are the same.

(5) The voltage drop in a tubular SOFC is caused by overpotential and contact resistance between tubular SOFCs. The overpotential consists of only ohmic overpotential because the ohmic overpotential is the largest one among the ohmic, activation, and concentration overpotentails in a tubular SOFC made by Siemens Westinghouse Power Corporation (SWPC) [10]. The logarithm

of the total resistance of the tubular SOFC, which is the summation of the anode, cathode, and electrolyte resistances, is expressed by a linear function of the inverse of the cell temperature because the logarithm of the cathode resistance, which is the largest one among three in the tubular SOFC made by SWPC [11], is expressed by a linear function of the inverse of the cathode temperature [12].

(6) Heat is only radiated from the combustor.
(7) All tubular SOFCs have the same characteristics in the SOFC stack.
(8) The average current density and oxygen utilization rate in the SOFC stack are the same as those in the tubular SOFC.

2.2. SOFC–PEFC system

The configuration of the SOFC–PEFC system is shown in Fig. 2. As mentioned above, the anode exhaust gas for the PEFC stack from the SOFC stack is supplied to the shift converter, and the exhaust gas from the shift converter is supplied to the CO selective oxidizer. The carbon monoxide in the anode exhaust gas for the PEFC stack from the SOFC stack is completely converted to carbon dioxide when the gas passes through the shift converter and the CO selective oxidizer. The exhaust gas from the CO selective oxidizer is supplied to the condenser, where the steam is captured as water by decreasing the temperature of the exhaust gas from the CO selective oxidizer. The exhaust gas from the condenser is supplied to the PEFC stack and hydrogen in the exhaust gas from the condenser is used for power generation. As mentioned above, the anode exhaust gas from the PEFC stack is distributed to each stack unit equally and burnt in the combustor of the stack unit. The combustion exhaust gas from the SOFC stack supplied to the heat exchanger is used for raising the temperature of the air supplied to the SOFC stack. The dc output of the SOFC stack and that of the PEFC stack are inverter-converted ac outputs. We call them gross ac outputs in this paper. Some of the gross ac outputs are used for the auxiliary machine for the SOFC stack and the one for the PEFC stack.

We used the following assumption for the simulation of the SOFC–PEFC system.

(1) Oxidation of hydrogen expressed as Eq. (3) is the only cell reaction in the PEFC stack [13].
(2) Ninety nine percent of the carbon monoxide in the anode exhaust gas from the SOFC stack is converted to carbon dioxide according to the shift reaction expressed as Eq. (2) in the shift converter.
(3) The carbon monoxide in the gas supplied to the CO selective oxidizer is completely oxidized to carbon dioxide. The only reaction that occurs in the CO selective oxidizer is the oxidation of carbon monoxide.

3. Fundamental equations

3.1. SOFC stack

The molar flow rate of methane fed to the pre-reformer, $M_{CH_4\text{-PRE-IN}}$, the molar flow rate of air supplied to the alumina tube, $M_{\text{A-ALM-IN}}$, the dc output of the tubular SOFC, W_{SO}, the molar flow rate of the anode exhaust gas for the PEFC stack, M_{APE}, and the molar flow rate of the combustion exhaust gas, M_{CEG}, are calculated using the average current density of the tubular SOFC, $J_{\text{SO-AVE}}$, the oxygen utilization rate of the SOFC stack, U_{oSOstack}, which is the same as that of the tubular SOFC, and the maximum temperature of the tubular SOFC, T_m, based on Eqs. (6)–(47). The $J_{\text{SO-AVE}}$ and T_m are 2000 A/m^2 [2] and 1273 K [14], respectively. The constants used in the simulation are listed in Table 1.

The temperature of the mixed gas supplied to the pre-reformer, $T_{\text{F-PRE-IN}}$, is calculated by

$$C_{CH_4} M_{CH_4\text{-PRE-IN}} (T_{\text{F-PRE-IN}} - T_{AMB}) = (T_{\text{F-SO-OUT}} - T_{\text{F-PRE-IN}}) \sum_i C_i M_{i\text{-REC}}, \quad (6)$$

where i represent methane, hydrogen, steam, carbon monoxide, and carbon dioxide.

The molar flow rate of methane at the pre-reformer outlet, $M_{CH_4\text{-PRE-OUT}}$, is calculated by [15]

$$M_{CH_4\text{-PRE-IN}} - M_{CH_4\text{-PRE-OUT}} = \kappa_{SR} V_p \exp\left(\frac{-\varepsilon_{SR}}{RT_{\text{F-PRE-IN}}}\right) p^{0.9845}_{CH_4\text{-PRE-IN}}. \quad (7)$$

The relationship between the equilibrium constant of shift reaction, K_{SHIF}, and the partial pressure of each gas component in the pre-reformer is expressed as

$$K_{SHIF}(T_{\text{F-PRE-OUT}}) = \frac{p_{CO_2\text{-PRE-OUT}} p_{H_2\text{-PRE-OUT}}}{p_{CO\text{-PRE-OUT}} p_{H_2O\text{-PRE-OUT}}}. \quad (8)$$

The mass and energy balance in the pre-reformer is expressed as

$$(M_{H_2O\text{-PRE-IN}} - M_{H_2O\text{-PRE-OUT}}) - (M_{CH_4\text{-PRE-IN}} - M_{CH_4\text{-PRE-OUT}}) + (M_{CO_2\text{-PRE-IN}} - M_{CO_2\text{-PRE-OUT}}) = 0, \quad (9)$$

$$(M_{H_2\text{-PRE-IN}} - M_{H_2\text{-PRE-OUT}}) + 3(M_{CH_4\text{-PRE-IN}} - M_{CH_4\text{-PRE-OUT}}) - (M_{CO_2\text{-PRE-IN}} - M_{CO_2\text{-PRE-OUT}}) = 0, \quad (10)$$

$$(M_{CO\text{-PRE-IN}} - M_{CO\text{-PRE-OUT}}) + (M_{CH_4\text{-PRE-IN}} - M_{CH_4\text{-PRE-OUT}}) + (M_{CO_2\text{-PRE-IN}} - M_{CO_2\text{-PRE-OUT}}) = 0, \quad (11)$$

Table 1
List of constants

Constant	Value
A_{COM} (m^2)	2.44×10^{-3}
A_{HE} (m^2)	10.7
C_{CH_4} (J/mol K)	61.9
C_{CO} (J/mol K)	31.8
C_{CO_2} (J/mol K)	50
C_{H_2} (J/mol K)	29.9
C_{H_2O} (J/mol K)	44
C_{N_2} (J/mol K)	31.4
C_{O_2} (J/mol K)	33.3
d_{ALM} (m)	1×10^{-3}
d_{ANO} (m)	1×10^{-4} [18]
d_{CATH} (m)	2.2×10^{-3} [18]
d_{ELE} (m)	4×10^{-5} [18]
d_{Wall} (m)	1×10^{-3}
F (C/mol)	96484
h_{COM} (W/m^2 K)	40 [19]
h_{HE} (W/m^2 K)	40 [19]
l_{CELL} (m)	1.2 [2]
l_{FCHA} (m)	5.2×10^{-3} [2]
$L_{oAUX\text{-}Pestack}$	0.93 [20]
L_{oBLOW}	0.04 [3]
L_{oOTHER}	0.03 [3]
N	1152 [2]
$N_{uA\text{-}ALM\text{-}INS}$	4.36 [16]
$N_{uA\text{-}ALM\text{-}OUTS}$	9.98 [16]
$N_{uA\text{-}CATH}$	7.19 [16]
N_{uF}	8.23 [16]
Q (W)	1.8×10^4 [2]
R_B ($\Omega\,m^2$)	1
R_c ($\Omega\,m^2$)	3.5×10^{-5} [2,18]
S_{SRE} (m^2)	1.15×10^{-4} [2]
T_{AMB} (K)	298
T_h (K)	1173
V_p (m^3)	1.08×10^{-5}
δ_{ALM} (m)	6.8×10^{-3}
δ_{SO} (m)	1.76×10^{-2}
$\Delta H_{CH_4\text{-}OXI}$ (J/mol)	-8.03×10^5
$\Delta H_{CO\text{-}OXI}$ (J/mol)	-2.82×10^5
$\Delta H_{H_2\text{-}OXI}$ (J/mol)	-2.49×10^5
ΔH_{SHIF} (J/mol)	-3.22×10^4
ΔH_{SR} (J/mol)	2.26×10^5
ε_{SR} (J/mol)	2.28×10^4 [15]
φ_{ALM} (m)	8.8×10^{-3}
φ_{SO} (m)	2.2×10^{-2} [18]
κ_{SR} (mol/(m^3/cat)s $MPa^{0.9845}$)	1.65 × 104 [15]
λ_A (W/m K)	0.078
λ_{ALM} (W/m K)	2.6 [21]
λ_{ANO} (W/m K)	6 [21]
λ_{CATH} (W/m K)	11 [21]
λ_{ELE} (W/m K)	2.7 [21]
λ_F (W/m K)	0.51
λ_{SRE} (W/m K)	6.28 [15]
ψ	0.94 [20]

and

$$-(T_{F\text{-}PRE\text{-}IN} - T_{F\text{-}PRE\text{-}OUT})\sum_i C_i M_{i\text{-}PRE\text{-}IN} + (M_{CH_4\text{-}PRE\text{-}IN} - M_{CH_4\text{-}PRE\text{-}OUT})\Delta H_{SR} - (M_{CO_2\text{-}PRE\text{-}IN} - M_{CO_2\text{-}PRE\text{-}OUT})\Delta H_{SHIF} = 0. \quad (12)$$

The energy balance in the fuel channel, wall 1, and wall 2 is expressed as

$$-\frac{\partial}{\partial x}\left\{\sum_i M_{i\text{-}FCHA\text{-}IN} C_i T_{F\text{-}FCHA}(x)\right\} - \varphi_{SO} h_{F\text{-}SRE}\{T_{F\text{-}FCHA}(x) - T_{Wall2}(x)\} = 0, \quad (13)$$

$$h_{F\text{-}SO}\{T_{F\text{-}SO}(x) - T_{Wall1}(x)\} + h_{F\text{-}SRE}\{T_{SRE}(x) - T_{Wall1}(x)\} + d_{Wall}\lambda_{ALM}\frac{\partial^2 T_{Wall1}(x)}{\partial x^2} = 0, \quad (14)$$

and

$$h_{F\text{-}SRE}\{T_{SRE}(x) - T_{Wall2}(x)\} + h_{F\text{-}SRE}\{T_{F\text{-}FCHA}(x) - T_{Wall2}(x)\} + d_{Wall}\lambda_{ALM}\frac{\partial^2 T_{Wall2}(x)}{\partial x^2} = 0, \quad (15)$$

where the heat transfer coefficient in the fuel channel and the stack reformer, $h_{F\text{-}SRE}$, and the heat transfer coefficient at the anode side of the tubular SOFC, $h_{F\text{-}SO}$, are [16]

$$h_{F\text{-}SRE} = \frac{\lambda_F N_{uF}}{2 l_{FCHA}}, \quad (16)$$

and

$$h_{F\text{-}SO} = \frac{\lambda_F N u_{uF}}{\varphi_{SO}}. \quad (17)$$

The molar flow rate in the stack reformer, $M_{CH_4\text{-}SRE}$, varies according to [15]

$$\frac{\partial M_{CH_4\text{-}SRE}(x)}{\partial x} = S_{SRE}\kappa_{SR}\exp\left(\frac{-\varepsilon_{SR}}{R T_{SRE}(x)}\right) \times p_{CH_4\text{-}SRE}(x)^{0.9845}. \quad (18)$$

The equilibrium constant of the shift reaction, K_{SHIF}, is expressed by

$$K_{SHIF}\{T_{SRE}(x)\} = \frac{p_{CO_2\text{-}SRE}(x)\,p_{H_2\text{-}SRE}(x)}{p_{CO\text{-}SRE}(x)\,p_{H_2O\text{-}SRE}(x)}, \quad (19)$$

using the partial pressure of each gas component in the stack reformer. The mass and energy balance in the stack reformer is expressed by

$$\frac{\partial M_{H_2O\text{-}SRE}(x)}{\partial x} - \frac{\partial M_{CH_4\text{-}SRE}(x)}{\partial x} + \frac{\partial M_{CO_2\text{-}SRE}(x)}{\partial x} = 0, \quad (20)$$

$$\frac{\partial M_{H_2\text{-}SRE}(x)}{\partial x} + 3\frac{\partial M_{CH_4\text{-}SRE}(x)}{\partial x} - \frac{\partial M_{CO_2\text{-}SRE}(x)}{\partial x} = 0, \quad (21)$$

$$\frac{\partial M_{CO\text{-}SRE}(x)}{\partial x} + \frac{\partial M_{CH_4\text{-}SRE}(x)}{\partial x} + \frac{\partial M_{CO_2\text{-}SRE}(x)}{\partial x} = 0, \quad (22)$$

and

$$-\frac{\partial}{\partial x}\left\{\sum_i M_{i\text{-SRE}}(x)C_i T_{\text{SRE}}(x)\right\} + \varphi_{\text{SO}} l_{\text{FCHA}}\lambda_{\text{SRE}}\frac{\partial^2 T_{\text{SRE}}(x)}{\partial x^2} - \{T_{\text{SRE}}(x) - T_{\text{h}}\} \times \left\{\sum_i C_i \frac{\partial M_{i\text{-SRE}}(x)}{\partial x}\right\} + \frac{\partial M_{\text{CH}_4\text{-SRE}}(x)}{\partial x}\Delta H_{\text{SR}} - \frac{\partial M_{\text{CO}_2\text{-SRE}}(x)}{\partial x}\Delta H_{\text{SHIF}} - \varphi_{\text{SO}} h_{\text{F-SRE}}\{T_{\text{SRE}}(x) - T_{\text{Wall1}}(x)\} - \varphi_{\text{SO}} h_{\text{F-SRE}}\{T_{\text{SRE}}(x) - T_{\text{Wall2}}(x)\} = 0. \quad (23)$$

The equilibrium constant of the oxidation of hydrogen, $K_{\text{H}_2\text{-OXI}}$, that of carbon monoxide, $K_{\text{CO-OXI}}$, and that of methane, $K_{\text{CH}_4\text{-OXI}}$, are expressed by

$$K_{\text{H}_2\text{-OXI}}\{T_{\text{F-SO}}(x)\} = \frac{p_{\text{H}_2\text{O-SO}}(x)}{p_{\text{H}_2\text{-SO}}(x)\{p_{\text{O}_2\text{-ANO}}(x)\}^{0.5}}, \quad (24)$$

$$K_{\text{CO-OXI}}\{T_{\text{F-SO}}(x)\} = \frac{p_{\text{CO}_2\text{-SO}}(x)}{p_{\text{CO-SO}}(x)\{p_{\text{O}_2\text{-ANO}}(x)\}^{0.5}}, \quad (25)$$

and

$$K_{\text{CH}_4\text{-OXI}}\{T_{\text{F-SO}}(x)\} = \frac{\{p_{\text{H}_2\text{O-SO}}(x)\}^2 p_{\text{CO}_2\text{-SO}}(x)}{p_{\text{CH}_4\text{-SO}}(x)\{p_{\text{O}_2\text{-ANO}}(x)\}^2}, \quad (26)$$

using the partial pressure of each gas component at the anode side of the tubular SOFC. The mass and energy balance at the anode side of the tubular SOFC is expressed by

$$\frac{\partial M_{\text{H}_2\text{O-SO}}(x)}{\partial x} + 2\frac{\partial M_{\text{CH}_4\text{-SO}}(x)}{\partial x} + \frac{\partial M_{\text{H}_2\text{-SO}}(x)}{\partial x} = 0, \quad (27)$$

$$\frac{\partial M_{\text{CO}_2\text{-SO}}(x)}{\partial x} + \frac{\partial M_{\text{CH}_4\text{-SO}}(x)}{\partial x} + \frac{\partial M_{\text{CO-SO}}(x)}{\partial x} = 0, \quad (28)$$

and

$$-\frac{\partial}{\partial x}\left\{\sum_i M_{i\text{-SO}}(x)C_i T_{\text{F-SO}}(x)\right\} + T_{\text{CELL-SO}}(x)\sum_i C_i \frac{\partial M_{i\text{-SO}}(x)}{\partial x} - \varphi_{\text{SO}} h_{\text{F-SO}}\{T_{\text{F-SO}}(x) - T_{\text{Wall1}}(x)\} - \varphi_{\text{SO}} h_{\text{F-SO}}\{T_{\text{F-SO}}(x) - T_{\text{CELL-SO}}(x)\} = 0. \quad (29)$$

The mass and energy balance at the cathode side of the tubular SOFC is expressed by

$$2\frac{\partial M_{\text{CH}_4\text{-SO}}(x)}{\partial x} + 0.5\frac{\partial M_{\text{H}_2\text{-SO}}(x)}{\partial x} + 0.5\frac{\partial M_{\text{CO-SO}}(x)}{\partial x} = \frac{\partial M_{\text{O}_2\text{-CATH}}(x)}{\partial x} \quad (30)$$

and

$$-\frac{\partial}{\partial x}\{M_{\text{O}_2\text{-CATH}}(x)C_{\text{O}_2}T_{\text{A-SO}}(x) + M_{\text{N}_2\text{-ALM-IN}}C_{\text{N}_2}T_{\text{A-SO}}(x)\} + C_{\text{O}_2}T_{\text{CELL-SO}}(x) \times \frac{\partial M_{\text{O}_2\text{-CATH}}(x)}{\partial x} - \pi\varphi_{\text{ALM}}h_{\text{A-ALM-OUTS}}\{T_{\text{A-SO}}(x) - T_{\text{ALM}}(x)\} - \pi\delta_{\text{SO}}h_{\text{A-CATH}}\{T_{\text{A-SO}}(x) - T_{\text{CELL-SO}}(x)\} = 0, \quad (31)$$

where the heat transfer coefficient between the air supplied to the cathode of the tubular SOFC and the cathode of the tubular SOFC, $h_{\text{A-CATH}}$, is given by

$$h_{\text{A-CATH}} = \frac{\lambda_{\text{A}} N_{\text{u}_{\text{A}}\text{-CATH}}\delta_{\text{SO}}}{\delta_{\text{SO}}^2 - \varphi_{\text{ALM}}^2}, \quad (32)$$

and the heat transfer coefficient between the air supplied to the cathode of the tubular SOFC and the alumina tube, $h_{\text{A-ALM-OUTS}}$, is given by

$$h_{\text{A-ALM-OUTS}} = \frac{\lambda_{\text{A}} N_{\text{uA-ALM-OUTS}}\varphi_{\text{ALM}}}{\delta_{\text{SO}}^2 - \varphi_{\text{ALM}}^2}, \quad (33)$$

The energy balance in the tubular SOFC is given by

$$\varphi_{\text{SO}}h_{\text{F-SO}}\{T_{\text{F-SO}}(x) - T_{\text{CELL-SO}}(x)\} + \pi\delta_{\text{SO}}h_{\text{A-CATH}} \times \{T_{\text{A-SO}}(x) - T_{\text{CELL-SO}}(x)\} - \{T_{\text{CELL-SO}}(x) - T_{\text{h}}\} \times \sum_i C_i \frac{\partial M_{i\text{-SO}}(x)}{\partial x} - \{T_{\text{CELL-SO}}(x) - T_{\text{h}}\} \times C_{\text{O}_2}\frac{\partial M_{\text{O}_2\text{-CATH}}(x)}{\partial x} + \frac{\partial M_{\text{CH}_4\text{-SO}}(x)}{\partial x}\Delta H_{\text{CH}_4\text{-OXI}} + \frac{\partial M_{\text{H}_2\text{-SO}}(x)}{\partial x}\Delta H_{\text{H}_2\text{-OXI}} + \frac{\partial M_{\text{CO-SO}}(x)}{\partial x}\Delta H_{\text{CO-OXI}} + \pi\varphi_{\text{SO}}(d_{\text{ANO}}\lambda_{\text{ANO}} + d_{\text{CATH}}\lambda_{\text{CATH}} + d_{\text{ELE}}\lambda_{\text{ELE}}) \times \frac{\partial^2 T_{\text{CELL-SO}}(x)}{\partial x^2} = \pi\varphi_{\text{SO}}J_{\text{SO}}(x)V_{\text{SO}}. \quad (34)$$

The current density of tubular SOFC, $J_{\text{SO}}(x)$, is given [17]

$$J_{\text{SO}}(x) = -\frac{4F}{\pi\varphi_{\text{SO}}}\frac{\partial M_{\text{O}_2\text{-CATH}}(x)}{\partial x}. \quad (35)$$

The voltage of the tubular SOFC, V_{SO}, is given by

$$V_{\text{SO}} = E_{\text{SO}}(x) - \phi_{\text{SO}}(x) - J_{\text{SO}}(x)R_{\text{c}}, \quad (36)$$

where the electromotive force of tubular SOFC, $E_{\text{SO}}(x)$, is calculated by the following Nernst equation [9]:

$$E_{\text{SO}}(x) = -\frac{RT_{\text{CELL-SO}}(x)}{4F}\ln\left\{\frac{p_{\text{O}_2\text{-ANO}}(x)}{p_{\text{O}_2\text{-CATH}}(x)}\right\}. \quad (37)$$

The ohmic overpotential of tubular SOFC, $\phi_{\text{SO}}(x)$, is given by

$$\phi_{\text{SO}}(x) = R_e\{T_{\text{CELL-SO}}(x)\}J_{\text{SO}}(x), \quad (38)$$

where the total resistance of the tubular SOFC, $R_{\text{e}}\{T_{\text{CELL-SO}}(x)\}$, which is the summation of the anode, cathode, and electrolyte resistances, is expressed by

$$R_e\{T_{\text{CELL-SO}}(x)\} = R_{\text{B}}\exp\left\{\frac{C_1}{T_{\text{CELL-SO}}(x)} + C_2\right\}, \quad (39)$$

where the values for C_1 and C_2 were estimated to be 5822 and −14.4, respectively. These values were estimated from the *I–V* characteristics of the tubular SOFC made by SWPC at 1173 and 1273 K [18], which had no voltage drop caused by the contact resistance. We assumed that voltage drop in the tubular SOFC made by SWPC consists of only ohmic overpotential when we estimated the values for C_1 and C_2.

The energy balance of the air flow inside the alumina tube and that of the alumina tube are expressed by

$$-\frac{\partial}{\partial x}\{M_{\text{A-SO-IN}}C_{\text{AIR}}T_{\text{A-ALM}}(x)\} - \pi\delta_{\text{ALM}}h_{\text{A-ALM-INS}} \times \{T_{\text{A-ALM}}(x) - T_{\text{ALM}}(x)\} = 0, \tag{40}$$

$$\pi\varphi_{\text{ALM}}h_{\text{A-ALM-OUTS}}\{T_{\text{A-SO}}(x) - T_{\text{ALM}}(x)\} + \pi\delta_{\text{ALM}}h_{\text{A-ALM-INS}}\{T_{\text{A-ALM}}(x) - T_{\text{ALM}}(x)\} + \pi d_{\text{ALM}}\varphi_{\text{ALM}}\lambda_{\text{ALM}}\frac{\partial^2 T_{\text{ALM}}(x)}{\partial x^2} = 0. \tag{41}$$

The heat transfer coefficient inside the alumina tube, $h_{\text{A-ALM-INS}}$, is given by

$$h_{\text{A-ALM-INS}} = \frac{\lambda_{\text{A}}N_{\text{u}_{\text{A}}\text{-ALM-INS}}}{\delta_{\text{ALM}}}. \tag{42}$$

The energy balance in the combustor is expressed by

$$\begin{aligned}
&-\Delta H_{\text{CH}_4\text{-OXI}}(M_{\text{CH}_4\text{-SO-OUT}} + M_{\text{CH}_4\text{-PEstack-OUT}}/N) \\
&- \Delta H_{\text{H}_2\text{-OXI}}(M_{\text{H}_2\text{-SO-OUT}} + M_{\text{H}_2\text{-PEstack-OUT}}/N) \\
&- \Delta H_{\text{CO}}M_{\text{CO-SO-OUT}} - Q/N \\
&= C_{\text{A}}M_{\text{A-ALM-IN}}(T_{\text{A-INS-ALM-COM-OUT}} - T_{\text{A-ALM-IN}}) \\
&\quad + C_{\text{O}_2}M_{\text{O}_2\text{-SO-OUT}}(T_{\text{CEG-COM}} - T_{\text{A-SO-OUT}}) \\
&\quad + C_{\text{N}_2}M_{\text{N}_2\text{-ALM-IN}}(T_{\text{CEG-COM}} - T_{\text{A-SO-OUT}}) \\
&\quad + \sum_i C_i M_{i\text{-SO-OUT}}(T_{\text{CEG-COM}} - T_{\text{F-SO-OUT}}) \\
&\quad + \sum_i C_i M_{i\text{-PEstack-OUT}}(T_{\text{CEG-COM}} \\
&\quad - T_{\text{F-PEstack-OUT}})/N,
\end{aligned} \tag{43}$$

where the air temperature inside the alumina tube at outlet of the combustor, $T_{\text{A-INS-ALM-COM-OUT}}$, is calculated by [19]

$$\begin{aligned}
&C_{\text{A}}M_{\text{A-ALM-IN}}(T_{\text{A-INS-ALM-COM-OUT}} - T_{\text{A-ALM-IN}}) \\
&= h_{\text{COM}}A_{\text{COM}} \\
&\quad \times \frac{(T_{\text{CEG-COM}} - T_{\text{A-ALM-IN}}) - (T_{\text{A-SO-OUT}} - T_{\text{A-INS-ALM-COM-OUT}})}{\ln\{(T_{\text{CEG-COM}} - T_{\text{A-ALM-IN}})/(T_{\text{A-SO-OUT}} - T_{\text{A-INS-ALM-COM-OUT}})\}}.
\end{aligned} \tag{44}$$

The molar flow rate of the combustion exhaust gas, M_{CEG}, is given by

$$\begin{aligned}
M_{\text{CEG}} = {} & (M_{\text{H}_2\text{O-SO-OUT}} + M_{\text{H}_2\text{O-PEstack-OUT}}/N) \\
& + (M_{\text{CO}_2\text{-SO-OUT}} + M_{\text{CO}_2\text{-PEstack-OUT}}/N) \\
& + (M_{\text{O}_2\text{-SO-OUT}} + M_{\text{N}_2\text{-SO-OUT}}) \\
& - 0.5(M_{\text{H}_2\text{-SO-OTU}} + M_{\text{H}_2\text{-PEstack-OUT}}/N) \\
& - 0.5M_{\text{CO-SO-OUT}}.
\end{aligned} \tag{45}$$

The dc output of the tubular SOFC, W_{SO}, is given by

$$W_{\text{SO}} = \pi\varphi_{\text{SO}}V_{\text{SO}}\int_0^{l\text{cell}} J_{\text{SO}}(x)\,\text{d}x. \tag{46}$$

The molar flow rate of the anode exhaust gas for the PEFC stack, M_{APE}, is given by

$$M_{\text{APE}} = M_{\text{AEG-SO}} - M_{\text{a}}. \tag{47}$$

The molar flow rate of the methane fed to the SOFC stack, $M_{\text{CH}_4\text{-SOstack-IN}}$, the molar flow rate of the air supplied to the SOFC stack, $M_{\text{A-SOstack-IN}}$, the dc output of the SOFC stack, $W_{\text{SOstack-dc}}$, the molar flow rate of the anode exhaust gas for PEFC stack from the SOFC stack, $M_{\text{APE-SOstack}}$, and the molar flow rate of the combustion exhaust gas from the SOFC stack, $M_{\text{CEG-SOstack}}$, are given by the following equations:

$$M_{\text{CH}_4\text{-SOstack-IN}} = M_{\text{CH}_4\text{-PRE-IN}}N, \tag{48}$$

$$M_{\text{A-SOstack-IN}} = M_{\text{A-ALM-IN}}N, \tag{49}$$

$$W_{\text{SOstack-dc}} = W_{\text{SO}}N, \tag{50}$$

$$M_{\text{APE-SOstack}} = M_{\text{APE}}N, \tag{51}$$

and

$$M_{\text{CEG-SOstack}} = M_{\text{CEG}}N. \tag{52}$$

3.2. SOFC–PEFC system

The dc output of the PEFC stack, $W_{\text{PEstack-dc}}$, is calculated from the fuel utilization rate of the PEFC stack, U_{fPEstack}, the voltage of the PEFC, V_{PE}, and the molar flow rate of the hydrogen in the exhaust gas from the CO selective oxidizer, $M_{\text{H}_2\text{-PEstack-IN}}$, using the following equation:

$$W_{\text{PEstack-dc}} = \frac{2M_{\text{H2-PEstack-IN}}U_{\text{fPEstack}}V_{\text{PE}}F}{100}, \tag{53}$$

where $M_{\text{H}_2\text{-PEstack-IN}}$ is given by

$$M_{\text{H}_2\text{-PEstack-IN}} = M_{\text{H}_2\text{-APE-SOstack}} + 0.99M_{\text{CO-APE-SOstack}}. \tag{54}$$

The temperature of the air supplied to the SOFC stack, $T_{\text{A-SOstack-IN}}$, is calculated based on the following equations:

$$C_{\text{A}}M_{\text{A-SOstack-IN}}(T_{\text{A-SOstack-IN}} - T_{\text{AMB}}) = C_{\text{COM}}M_{\text{CEG-SOstack}}(T_{\text{CEG-SO-OUT}} - T_{\text{CEG-HE-OUT}}). \tag{55}$$

and

$$C_{\text{A}}M_{\text{A-SOstack-IN}}(T_{\text{A-SOstack-IN}} - T_{\text{AMB}}) = K_{\text{HE}}A_{\text{HE}}\frac{(T_{\text{CEG-SO-OUT}} - T_{\text{A-SOstack-IN}}) - (T_{\text{CEG-HE-OUT}} - T_{\text{AMB}})}{\ln\{(T_{\text{CEG-SO-OUT}} - T_{\text{A-SOstack-IN}})/(T_{\text{CEG-HE-OUT}} - T_{\text{AMB}})\}}. \tag{56}$$

The ac output of the SOFC stack, $W_{\text{SOstack-ac}}$, and that of the PEFC stack, $W_{\text{PEstack-ac}}$, are given by

$$W_{\text{SOstack-ac}} = \psi(1 - L_{\text{oAUX-SOstack}})W_{\text{SOstack-dc}}, \quad (57)$$

and

$$W_{\text{PEstack-ac}} = \psi(1 - L_{\text{oAUX-PEstack}})W_{\text{PEstack-dc}}, \quad (58)$$

where the ratio of the power consumption in the auxiliary machine to the gross ac output of the SOFC stack, $L_{\text{oAUX-SOstack}}$, is calculated by

$$L_{\text{oAUX-SOstack}} = \frac{25L_{\text{oBLOW}}}{U_{\text{oSOstack}}} + L_{\text{oOTHER}}. \quad (59)$$

The ac output of the SOFC–PEFC system, W_{SYS}, and the electrical efficiency, η, are calculated by

$$W_{\text{SYS}} = W_{\text{SOstack-ac}} + W_{\text{PEstack-ac}}, \quad (60)$$

and

$$\eta = -\frac{100(W_{\text{PEstack-ac}} + W_{\text{SOstack-ac}})}{M_{\text{CH}_4\text{-SOstack-IN}}\Delta H_{\text{CH}_4\text{-OXI}}}. \quad (61)$$

4. Results and discussion

4.1. Effectiveness of simulation

The ac output and the electrical efficiency of the SOFC cogeneration system made by SWPC were simulated by using the simulation model shown in Fig. 1. We compared the simulation result with the actual performance demonstrated by SWPC [2] (see Table 2). The former is in good agreement with the later. We can conclude that our simulation is effective at estimating ac output and electrical efficiency.

4.2. Effect of oxygen utilization rate in the SOFC stack

The dependence of the ac outputs of the SOFC stack, the PEFC stack, and the SOFC–PEFC system on the oxygen utilization rate in the SOFC stack is shown in Fig. 3. The maximum temperature in the SOFC stack is less than 1273 K when the oxygen utilization rate in the SOFC stack is less than 30%, because a large amount of exhaust heat of the SOFC stack is discharged from the stack when a large amount of air supplied to the SOFC stack. The methane with a molar flow rate exceeding the molar flow rate needed to keep the average current density of the tubular SOFC at 2000 A/m^2 is reformed in the stack reformer while the maximum temperature in the SOFC stack is maintained at

Table 2
Comparison of ac output and electrical efficiency

	ac output (kW)	Electrical efficiency(%)
Simulation	114	47
SWPC [2]	109	46

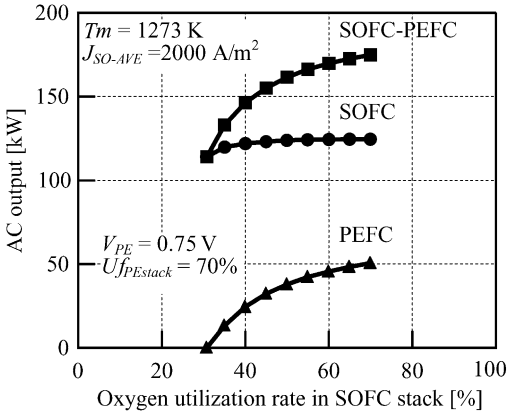

Fig. 3. Dependence of ac outputs of the SOFC stack, PEFC stack, and SOFC–PEFC system on the oxygen utilization rate in the SOFC stack. T_{m}: maximum temperature in SOFC stack, $J_{\text{SO-AVE}}$: average current density in SOFC stack, V_{PE}: cell voltage in PEFC stack and U_{fPEstack}: fuel utilization rate in PEFC stack.

1273 K when the oxygen utilization in the SOFC stack is over 30%. This is because the amount of exhaust heat of the SOFC stack discharged with the air decreases with increasing oxygen utilization rate in the SOFC stack and because that used effectively as the reaction heat of the steam reforming reaction of methane in the stack reformer increases. The ac output of the PEFC stack increases with increasing oxygen utilization rate in the SOFC stack because the methane used for the power generation of the PEFC stack increases. The ac output of the SOFC stack slightly increases with increasing oxygen utilization rate in the SOFC stack. This is because the cell voltage of the tubular SOFC increases since the partial pressures of hydrogen and carbon monoxide in the steam-reformed gas at the anode of the tubular SOFC increase, and because the power consumption of the air blower decreases. Consequently, the ac output of the SOFC–PEFC system, which is the sum of the ac outputs of SOFC and PEFC stacks, increases with increasing oxygen utilization rate in the SOFC stack. The amount of steam in the recycled gas for the steam reforming is insufficient and the S/C ratio in the mixed gas fed to the pre-reformer is less than 3.0 when the oxygen utilization rate in the SOFC stack is more than 70%. The ac output of the SOFC–PEFC system is 175 kW when the oxygen utilization rate in the SOFC stack is 70%.

The dependence of the electrical efficiency of the SOFC–PEFC system on the oxygen utilization rate in the SOFC stack is shown in Fig. 4. The electrical efficiency of the SOFC–PEFC system increases with increasing oxygen utilization rate in the SOFC stack. This is because the amount of exhaust heat of the SOFC stack used as the reaction heat of the steam reforming reaction increases and because that discharged from the stack with the air decreases. The electrical efficiency of the SOFC–PEFC system is 54% when the oxygen utilization rate in the SOFC stack is 70%. This value is far higher than the electrical efficiency at 109 kW ac of the SOFC cogeneration system demonstrated

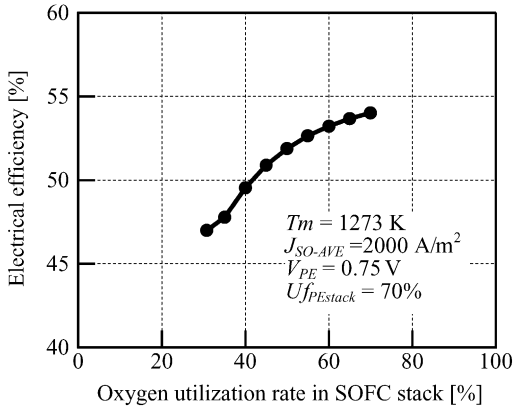

Fig. 4. Dependence of the electrical efficiency of the SOFC–PEFC system on the oxygen utilization rate in SOFC stack. T_m: maximum temperature in SOFC stack, $J_{SO\text{-}AVE}$: average current density in SOFC stack, V_{PE}: cell voltage in PEFC stack and $U_{fPEstack}$: fuel utilization rate in PEFC stack.

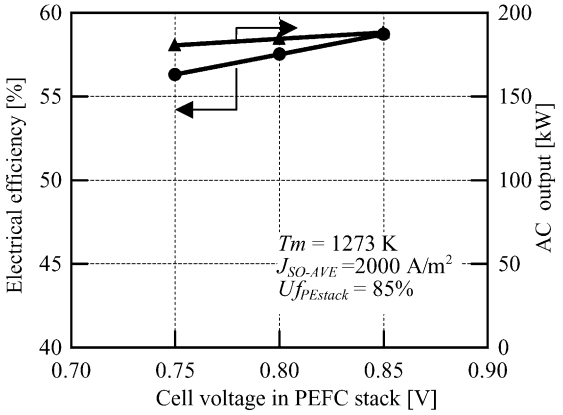

Fig. 6. Dependence of the electrical efficiency and ac output of the SOFC–PEFC system on cell voltage in the PEFC stack. T_m: maximum temperature in SOFC stack, $J_{SO\text{-}AVE}$: average current density in SOFC stack and $U_{fPEstack}$: fuel utilization rate in PEFC stack.

by SWPC, 46% [2], but lower than that at 220 kW ac of the SOFC–GT system designed by SWPC, 57% [4].

4.3. Effect of fuel utilization rate and cell voltage in PEFC stack

The fuel utilization rate of the PEFC stack in a PEFC system is low because the large amount of hydrogen in anode exhaust gas has to be burnt to generate the heat needed for the steam reforming reaction of methane and steam generation [22]. On the other hand, the fuel utilization rate of the PEFC stack in the SOFC–PEFC system can be increased compared with the PEFC system, because the temperature of the exhaust heat from the SOFC stack is about 1273 K and this heat can be used for the steam reforming reaction of methane and steam generation. The dependence of the electrical efficiency and the ac output of the SOFC–PEFC system on the fuel utilization rate in the PEFC stack is shown in Fig. 5. The electrical efficiency and the ac output of the SOFC–PEFC system increase with increasing fuel utilization rate in the PEFC stack. The electrical efficiency and the ac output of the SOFC–PEFC system are 56% and 180 kW, respectively, when the fuel utilization rate in the PEFC stack is 85%. The electrical efficiency of 56% is almost equal to that at 220 kW ac of the SOFC–GT system designed by SWPC, which is 57%.

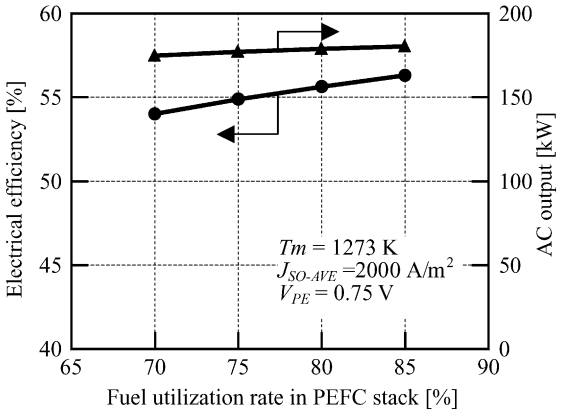

Fig. 5. Dependence of the electrical efficiency and ac output of the SOF–PEFC system on the fuel utilization rate in PEFC stack. T_m: maximum temperature in SOFC stack, $J_{SO\text{-}AVE}$: average current density in SOFC stack and V_{PE}: cell voltage in PEFC stack.

The dependence of the electrical efficiency and the ac output of the SOFC–PEFC system on the cell voltage in the PEFC stack is shown in Fig. 6. The electrical efficiency and ac output of the SOFC–PEFC system increase with the cell voltage in the PEFC stack. The electrical efficiency and ac output of the SOFC–PEFC system are 59% and 190 kW, respectively, when the cell voltage in the PEFC stack is 0.85 V. The electrical efficiency of 59% is equal to that at 1014 kW ac of the SOFC–GT system designed by SWPC [4].

5. Summary

We evaluated the 200 kW-class SOFC–PEFC system by numerical simulation. The main results are as follows.

1. The electrical efficiency of the SOFC–PEFC system increases with increasing oxygen utilization rate in the SOFC stack. This is because the amount of exhaust heat of the SOFC stack discharged from the SOFC stack with the supplied air decreases as the oxygen utilization rate in the SOFC stack increases and because that used effectively as the reaction heat of the steam reforming reaction of methane in the stack reformer increases.
2. The electrical efficiency at 190 kW ac of the SOFC–PEFC system is 59% when the fuel utilization rate and the cell voltage in the PEFC stack are 85% and 0.85 V, respectively. This electrical efficiency is equal to that of the SOFC–GT system at 1014 kW ac.

References

[1] J. Larminie, A. Dicks, Fuel Cell Systems Explained, Wiley, 2000, pp. 123–134.
[2] R.A. George, J. Power Source 86 (2000) 134–139.
[3] S.E. Veyo, W.L. Lundberg, in: Proceedings of the International Gas Turbine and Aeroengine Congress and Exhibition, 1999, paper 99-GT-550.
[4] S.E. Veyo, L.A. Shockling, J.T. Dedere, J.E. Gillett, W.L. Lundberg, in: Proceedings of the Interna Gas Turbine and Aeroengine Congress and Exhibition, 2000, paper 2000-GT-550.
[5] H.E. Vollmar, C.U. Maier, C. Nolscher, T. Merklein, M. Poppinger, J. Power Source 86 (2000) 90–97.
[6] A.L. Dicks, R.G. Fellows, C.M. Mescal, C. Seymour, J. Power Source 86 (2000) 501–506.
[7] W.L. Lundberg, in: Proceedings of the Symposium on Fuel Cells, 1989, pp. 118–129.
[8] T. Iwanari, N. Miyauchi, K. Ito, K. Onda, Y. Sakaki, S. Nagata, Trans. Jpn. Soc. Mechanical Eng., Ser. B 68 (673) (2002) 214–220 (in Japanese).
[9] S. Nagata, Y. Kasuga, Y. Ono, Y. Kaga, H. Sato, Trans. Inst. Electrical Eng. Jpn. 107 (B-3) (1982) 147–154 (in Japanese).
[10] N.J. Masakalick, in: Proceedings of the First International Symposium on Solid Oxide Fuel Cells, 1989, pp. 279–287.
[11] K. Kinoshita, F.R. McLarnon, E.J. Cairns, Fuel Cells, A Handbook, US Department of Energy, Office of Fossil Energy, 1988, pp. 87–104.
[12] J.H. Kuo, H.U. Anderson, D.M. Sparlin, J. Solid State Chem. 87 (1990) 55–63.
[13] L.J.M.J. Blomen, M.N. Mugerwa, Fuel Cell Systems, Plenum Press, 1993, pp. 493–495.
[14] S.E. Veyo, Fuel Cell Seminar Abstracts, 1998, pp. 457–461.
[15] T. Take, T. Yamashita, M. Tomura, J. Chem. Eng. Jpn. 33 (2000) 67–77.
[16] The Japan Society of Mechanical Engineers, JSME Data Book: Heat Transfer, Fourth ed., The Japan Society of Mechanical Engineers, 1986, pp. 50–52 (in Japanese).
[17] E. Erdle, J. Groos, H.G. Muller, W.J.C. Muller, R. Sonnenschein, Report of EUR 13158 EN, Commission of the European Communities, 1991.
[18] S.C. Singhal, Solid Oxide Fuel Cell V, Electrochem. Soc. Proc. 97 (18) (1997) 37–50.
[19] The Japan Society of Mechanical Engineers, JSME Data Book: Heat Transfer, Fourth ed., The Japan Society of Mechanical Engineers, 1986, pp. 244–248 (in Japanese).
[20] A. Sonai, K. Sakai, K. Tanaka, A. Kano, H. Nishikawa, Trans. Inst. Electrical Eng. Jpn. 122 (B-8) (2002) 938–943 (in Japanese).
[21] S. Nagata, Y. Kasuga, A. Monma, T. Kato, Trans. Inst. Electrical Eng. Jpn. 116-B (1996) 918–924 (in Japanese).
[22] Y. Cao, Z. Guo, J. Power Source 109 (2002) 287–293.